

# Thermal Permeability Enhancement of Blocky Rocks: One-Dimensional Flows

D. ELSWORTH†

*A conceptual model is presented to describe permeability enhancement within competent blocky rock masses subjected to temperature changes. The model accommodates a ubiquitously jointed, isothermal and initially stressed mass into which fluid of a different temperature is injected. The transient behaviour of the coupled fluid flow and transport system is described using a 1-D or radial upwind weighted, conductive-advective transport model. Heat production from, and thermal volume change of, the surrounding matrix blocks is described analytically via a convolution product with individual blocks represented as equivalent spheres. The assumption of full lateral restraint for control volumes within the blocky mass results in stress redistribution not being explicitly represented. No attempt is made to satisfy stress equilibrium conditions. The model is used to identify the manner and rate at which fluid permeability enhancement processes develop within a representative granite rock mass. Thermal effects are shown to be significant.*

## INTRODUCTION

Hydraulic permeability enhancement has been an observed factor in many geothermal and hot dry rock energy recovery schemes [1] resulting in decreased flow impedance as reservoir development proceeds. The mechanisms by which this behaviour is effected results from a complex interaction of transient reservoir pressure, temperature and deformation response to the injected fluid disturbance. Increased *fluid pressures* within a minimally permeable and initially fractured rock mass will result in joint opening [2], shear deformation and bridging [3] and under more extreme conditions crack extension. Since the fluid permeability of single fractures is proportional to aperture raised to the power three, small dilatant deformations may greatly increase formation permeability. Sudden, non-uniform or cyclic *temperature changes* may overstress the intact rock and result in increased fracture density of cracks at both the micro- and macro-scales [4]. Additionally, *transient cooling* of the rock mass will induce contractile volumetric strain that may generate an increase in pre-existing macro-fracture volume even in the absence of new crack formation. The behaviour of the reservoir under this mode of thermal loading is determined primarily by the redistribution of thermal strains and *in situ* stresses that will result from quenching. Indeed, transient reductions in flow impedance within reservoirs producing at quasi-

constant rate are most likely attributed to this phenomenon.

The following addresses a simplified treatment of the behaviour of a hot rock reservoir containing a pre-existing ubiquitous, orthogonal fracture system. The treatment describes the transient development of rock joint deformations that result from changes in fluid pressure and thermal straining within an initially stressed formation. The cornerstone of the analysis is the assumption that the jointed rock mass may be represented as a two-phase continuum comprising solid rock blocks separated by fluid filled discontinuities. Advective transport operates within the pre-existing fracture system with conductive transfer being the dominant mechanism governing thermal transfer between non-porous rock blocks and the fracture fluid.

Rock mass displacements and stresses are not explicitly accommodated. Rather, transient thermal volumetric strains are evaluated under the assumption that a macroscopic control volume containing an assemblage of rock blocks will remain at constant volume. Volume changes are therefore restricted to within the solid phase. For both heat production from the intact rock blocks and volumetric deformation of the mass, an analytical transfer function is used to accurately gauge the unsteady behaviour and determine the magnitude of permeability enhancement.

## GOVERNING EQUATIONS

The coupled equations describing the transient hydrothermal behaviour of a fluid saturated and ubiqui-

†Department of Mineral Engineering, The Pennsylvania State University, University Park, PA 16802, U.S.A.; currently at Waterloo Centre for Groundwater Research, University of Waterloo, Waterloo, Ontario, Canada N2L 3G1.

tously jointed rock mass are those for conservation of mass (the flow equation) and conservation of energy (heat transport equation). For radial flow within the horizontal plane, these may be stated as, respectively:

$$\frac{K_f}{\gamma_f} \frac{1}{r} \frac{\partial}{\partial r} \left( r \frac{\partial P_f}{\partial r} \right) + \rho_f q_e = \phi \beta_f \frac{\partial P_f}{\partial t}, \quad (1)$$

$$\left( \frac{D_f}{\phi} \right) \frac{1}{r} \frac{\partial}{\partial r} \left( r \frac{\partial T_f}{\partial r} \right) - \rho_f c_f \left( \frac{q_f}{\phi} \right) \frac{\partial T_f}{\partial r} + q_s = \rho_f c_f \frac{\partial T_f}{\partial t}, \quad (2)$$

where subscript f denotes fluid parameters, subscript s denotes terms pertaining to the solid (rock) phase and

- $T_f$  = fluid temperature,
- $P_f$  = fluid pressure,
- $K_f$  = hydraulic conductivity of fracture system,
- $D_f$  = thermal conductivity of fluid,
- $c_f$  = specific heat capacity of fluid,
- $q_e$  = externally supplied hydraulic flux,
- $q_f$  = total hydraulic flux (per unit volume),
- $\rho_f$  = fluid density,
- $\gamma_f$  = fluid unit weight,
- $\phi$  = fracture porosity of ubiquitously jointed mass,
- $\beta_f$  = fluid compressibility,
- $q_s$  = thermal flux from solid phase (per unit volume),
- $r$  = radial coordinate.

These equations may be readily transformed for the plane flow case. The equations are coupled in that the magnitude of the advective heat flux term of equation (2) is directly dependent on the solution of equation (1). Flow within the rock mass is controlled by temperature dependent fluid viscosity and the ability of single fractures to transmit fluid is strongly controlled by the fracture aperture ( $b$ ).

Although not explicitly represented in the heat transport or flow equations, changes in fracture apertures may be effected by modification in the fluid pressure regime or as the result of thermal straining within the matrix blocks. The effects of fluid pressures and thermal strains on the stress and displacement regime at the block surfaces may be accommodated under the assumption of full lateral restraint. Under this assumption, displacements between adjacent fracture walls may be determined directly from the known fluid pressures present within the fracture network and from the calculated thermal history at block faces. If the thermal history of individual block faces may be determined, the induced thermal stress and thermal displacement histories may also be evaluated.

### TRANSFER FUNCTIONS

Two transfer functions are required to supplement equations (1) and (2). The first is to represent the thermal contraction or expansion of individual blocks under a changing surface temperature regime. This displacement will directly affect the magnitude of the hydraulic conductivity term ( $K_f$ ) in equation (1). The second transfer function is required to accurately describe the thermal flux stimulated from the block as it is cooled or warmed

from ambient temperature. This thermal energy will be transferred directly to the advecting fluid through  $q_s$  in equation (2). To maintain the problem definition at a tractable level, individual rock blocks are represented as equivalent spheres. This concept together with the rock mass geometry is illustrated in Fig. 1.

#### 1. Block surface displacement

For an unstressed spherical block of radius  $a$ , coefficient of thermal expansion  $\alpha_s$  and with a radial temperature distribution within the solid material  $T_r$ , the displacement at any radius  $r$  may be given as [5]:

$$u_r = \alpha_s \left( \frac{3\lambda + 2\mu}{\lambda + 2\mu} \right) \left\{ \frac{1}{r^2} \int_0^r T_r r^2 dr + \frac{4\mu}{(3\lambda + 2\mu)} \left( \frac{r}{a^3} \right) \int_0^a T_r r^2 dr \right\}, \quad (3)$$

where  $\lambda$  and  $\mu$  are Lamé coefficients. Although, in general, the temperature distribution within the block will be a complex function of the external thermal loading history, the only specific interest in the context of this work is the boundary displacement. This displacement will control volumetric strain within the fractured medium. The surface block displacement,  $u_a$ , is therefore:

$$u_a = \frac{3\alpha_s}{a^2} \int_0^a T_r r^2 dr, \quad (4)$$

which, in a thermally equilibrated block at constant radial temperature  $T_r$ , above initial ambient, results in a surface displacement of  $u_a = \alpha_s T_r a$ .

The temporal and spatial variation in temperature within a spherical block, warmed or cooled at the boundary from ambient temperature may be obtained by solving the spherically symmetric initial value problem subject to the boundary conditions:

$$T_r = 0 \quad a > r > 0 \quad \text{for } t = 0^-, \quad (5)$$

$$T_r = T_a \quad r = a \quad \text{for } t > 0^+. \quad (6)$$

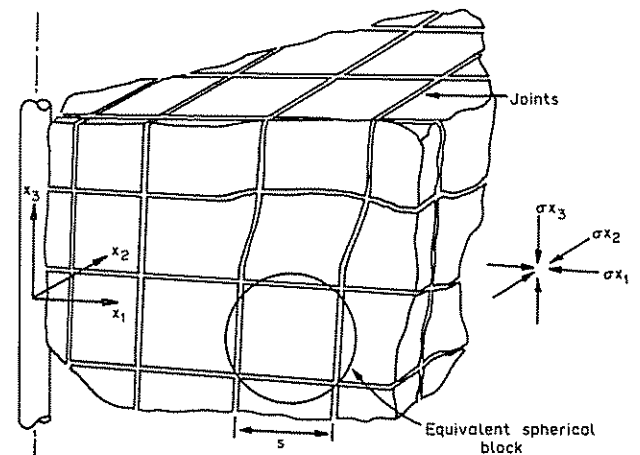


Fig. 1. Schematic geometry of a block jointed mass. Three orthogonal joint sets are present, each of equal spacing ( $s$ ). Field stresses act normal to joint sets.

Solution is available as [6]:

$$T_r^i = T_a + \frac{2aT_a}{\pi r} \sum_{n=1}^{\infty} \frac{(-1)^n}{n} \sin\left(\frac{n\pi r}{a}\right) \times \exp(-D_s n^2 \pi^2 t / \rho_s c_s a^2), \quad (7)$$

where  $D_s$  = solid phase thermal conductivity,  $\rho_s$  = solid phase density,  $c_s$  = solid phase specific heat capacity and the temperatures are determined at all radial locations ( $r$ ) and at all times ( $t$ ). Substituting equation (7) into equation (4) and performing the integration yields:

$$u_a^i = \alpha_s a T_a \left\{ 1 - \frac{6}{\pi^2} \sum_{n=1}^{\infty} \frac{1}{n^2} \exp(-D_s n^2 \pi^2 t / \rho_s c_s a^2) \right\}, \quad (8)$$

to give  $u_a^i$  = block surface displacement at time  $t$  resulting from a step temperature change ( $T_a$ ) applied at the outer boundary. This may be represented in dimensionless form as illustrated in Fig. 2 to give the block response as a unique function of dimensionless time  $D_s t / \rho_s c_s a^2$ . For a continuously varying applied thermal boundary condition ( $T_a^i$ ) the time dependent surface displacement may be obtained from use of a convolution product via Duhamel's Theorem [6].

For the specific case of equation (8):

$$u_a^i = \alpha_s a \int_0^i \frac{\partial T_a}{\partial t} \left\{ 1 - \frac{6}{\pi^2} \sum_{n=1}^{\infty} \frac{1}{n^2} \exp(\xi(t - \tau)) \right\} d\tau, \quad (9)$$

where

$$\xi = -D_s n^2 \pi^2 / \rho_s c_s a^2.$$

In general, the variation of temperature will not be known as a continuous function of time but will be evaluated only at the close of finite time increments  $\Delta t$ . Finite representation of the partial differential of equation (11) yields a series expansion:

$$\begin{aligned} u_a^{i+1} &\cong \alpha_s a \frac{\Delta T_a^i}{\Delta t^i} \\ &\times \int_{t_0}^{t_1} \left\{ 1 - \frac{6}{\pi^2} \sum_{n=1}^{\infty} \frac{1}{n^2} \exp(\xi(t^{i+1} - \tau)) \right\} d\tau \\ &+ \alpha_s a \frac{\Delta T_a^i}{\Delta t^i} \int_{t_1}^{t_2} \left\{ 1 - \frac{6}{\pi^2} \sum_{n=1}^{\infty} \frac{1}{n^2} \right. \\ &\times \exp(\xi(t^{i+1} - \tau)) \left. \right\} d\tau \\ &+ \dots + \alpha_s a \frac{\Delta T_a^{i+1}}{\Delta t^{i+1}} \\ &\times \int_{t^i}^{t^{i+1}} \left\{ 1 - \frac{6}{\pi^2} \sum_{n=1}^{\infty} \frac{1}{n^2} \exp(\xi(t^{i+1} - \tau)) \right\} d\tau \end{aligned} \quad (10)$$

with

$$\frac{\Delta T_a^{i+1}}{\Delta t^{i+1}} = \frac{T_a^{i+1} - T_a^i}{t^{i+1} - t^i}. \quad (11)$$

Performing the integration of equation (10) at the two time steps of  $t^i$  and  $t^{i+1}$  allows the displacement at the latter time level ( $u_a^{i+1}$ ) to be evaluated from the displace-

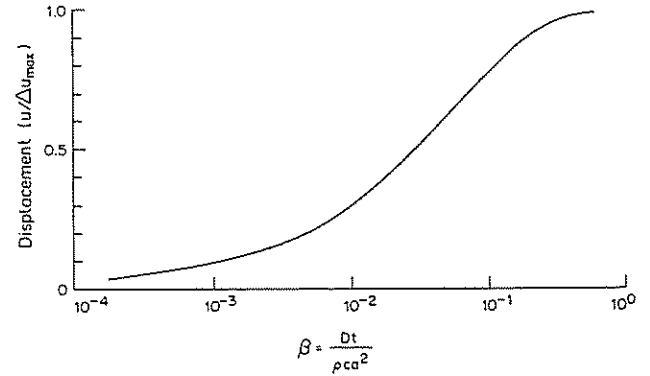


Fig. 2. Dimensionless displacement of a spherical block as a function of dimensionless time.

ment at the previous time level ( $u_a^i$ ). This is determined by the relation:

$$u_a^{i+1} = A_1^{i+1} + A_2^{i+1}, \quad (12)$$

$$A_1^{i+1} = A_1^i + \alpha_s \Delta T^{i+1}, \quad (13)$$

$$\begin{aligned} A_2^{i+1} &= \sum_{n=1}^{\infty} A_2^i \exp(\xi \Delta t^{i+1}) \\ &+ \alpha_s \frac{\Delta T^{i+1}}{\Delta t^{i+1}} \frac{6}{\pi^2} \sum_{n=1}^{\infty} \frac{1}{n^2 \xi} \\ &\times (1 - \exp(\xi \Delta t^{i+1})). \end{aligned} \quad (14)$$

This allows surface displacement to be determined due to any quantified history of surface temperatures in a sphere initially at a datum temperature.

## 2. Block surface heat flux

A similar procedure to the previous may be followed to determine heat flux transfer [7,8] from the surface of the spherical blocks as a function of time. Solution of the spherical heat flow, initial value problem is reported in equation (7). Thermal flux ( $f_s$ ) at the sphere boundary is given as:

$$f_s = -D_s \frac{\partial T}{\partial r} \Big|_{r=a}, \quad (15)$$

which on substituting equation (7) yields flux per unit surface area as:

$$f_s = -\frac{2D_s T_a}{a} \sum_{n=1}^{\infty} \exp(\xi t). \quad (16)$$

The flux per unit volume ( $q_s$ ) is given as:

$$q_s = f_s \cdot \frac{4\pi a^2}{(4/3)\pi a^3} = f_s \cdot \frac{3}{a}, \quad (17)$$

which upon using Duhamel's Theorem yields the volumetric rate of heat production ( $q_s$ ) as:

$$q_s^{i+1} = B_1^{i+1} \Delta T^{i+1} + B_2^{i+1}, \quad (18)$$

$$B_1^{i+1} = \frac{6D_s}{a^2 \Delta t^{i+1}} \sum_{n=1}^{\infty} \frac{1}{\xi} \{1 - \exp(\xi \Delta t^{i+1})\}, \quad (19)$$

$$B_2^{i+1} = \sum_{n=1}^{\infty} q_s^i \exp(\xi \Delta t^{i+1}). \quad (20)$$

It must be observed that both the displacement ( $u_a$ ) and heat flux ( $q_a$ ) terms are functions of infinite exponential series. The convergence of these series are particularly poor for small values of the coefficient  $D_s \Delta t / \rho_s c_s a^2$ . If, however, the time step increment ( $\Delta t$ ) is retained constant then the terms of the exponential series of equations (14), (19) and (20) are also constant with time and need only be evaluated once. More onerous than this is the requirement that the values of  $A_1^1$  [equation (14)] and  $B_1^1$  [equation (20)] be stored for each spatial evaluation of  $u_a^1$  or  $q_a^1$  and for each of the  $n$  terms of the truncated series. In the parametric studies reported in the following, the number of terms required to yield at least a 0.1% accuracy in the determination of both  $u_a^1$  and  $q_a^1$  were ten.

### INDUCED THERMAL POROSITY CHANGE

For considerations of equivalent total thermal energy it is necessary that the idealized spherical block and real cubic rock block illustrated in Fig. 1 have identical volumes. Consider a rock mass with ubiquitous orthogonal joint sets of uniform spacing ( $s$ ) and hence frequency ( $\lambda$ ) of 1/sec. The equivalent spherical radius ( $a$ ) may be equated as:

$$a = \left( \frac{3}{4\pi} \right)^{1/3} s. \quad (21)$$

For infinitesimal radial displacement on the surface of this sphere of ( $\Delta u$ ) the resulting volumetric strain ( $\Delta v/v$ ) of the sphere and hence the rock mass is obtained from the corollary of equations (17) and equation (21) as:

$$\frac{\Delta v}{v} = \frac{3\Delta u_a}{a} = \frac{-3}{s} \left( \frac{4\pi}{3} \right)^{1/3} \Delta u_a, \quad (22)$$

where contractile strains, compressive stresses and outward radial displacements are defined positive.

Assuming that in a cooling block, all deformations are uniform within the three orthogonal directions, contractile volume strain may be distributed equally between aperture enlargements on joint sets normal to the orthogonal axes. Total fracture area ( $a_f$ ) in a control volume  $dx$ , on edge is:

$$a_f = \frac{3}{s} dx_1 dx_2 dx_3, \quad (23)$$

the potential change in aperture ( $\Delta u_j$ ) will be:

$$\Delta u_j = \frac{-\Delta v}{v} \frac{dx_1 dx_2 dx_3}{a_f} \quad (24)$$

and on substituting equations (22) and (23) into (24) gives potential aperture change ( $\Delta u_j$ ) as:

$$\Delta u_j = \left( \frac{4\pi}{3} \right)^{1/3} \Delta u_a \cong 1.612 \Delta u_a. \quad (25)$$

This gives the potential for aperture enhancement ( $\Delta u_j$ ) of existing fractures in an initially *unstressed* medium. For a rock mass under homogenous triaxial initial stress  $\sigma_j$ , as illustrated in Fig. 1, displacements induced by changes in joint fluid pressure ( $\Delta p$ ) or

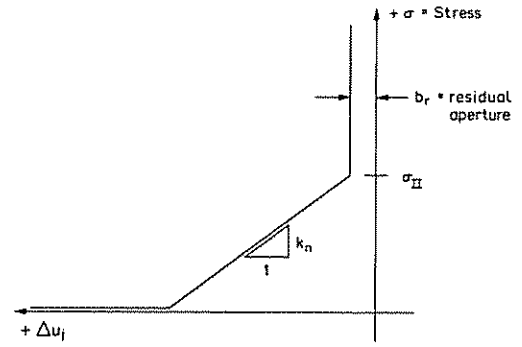


Fig. 3. Trilinear compression curve for a single rock joint. Normal stresses ( $\sigma$ ) are denoted as positive in compression,  $\sigma_{II}$  is the stress required to achieve maximum joint closure ( $b_r$ ). Joint aperture change ( $\Delta u_j$ ) is denoted positive in opening.

changes in thermal stress ( $\Delta \sigma_T$ ) will be moderated by both the *in situ* stress field and nonlinear joint stiffness. Considering only normal displacements, the trilinear joint compression curve illustrated in Fig. 3 is used. Assuming that each control volume of edge dimension  $dx_1 dx_2 dx_3$  remains constant and that blocks initially present within one volume may not migrate into adjacent volumes (i.e. full lateral and vertical restraint), then induced joint displacement ( $\Delta u_j$ ) under isothermal loading may be given as:

$$\Delta u_j = - \left[ \frac{E}{s(1-2\nu)} + k_n \right]^{-1} \Delta p, \quad (26)$$

where  $k_n$  = joint normal stiffness as defined in Fig. 3 and  $s \gg b$  where  $b$  = joint aperture. Fluid pressure is assumed to act uniformly on all faces of the block.

For the non-isothermal case, block surface ( $\Delta u_b$ ) and joint displacements are clearly related if it is mandated that the control volume ( $dx_1 dx_2 dx_3$ ) remain constant. Thus, for compatibility:

$$\Delta u_b + \Delta u_j = 0, \quad (27)$$

where

$$\Delta u_b = s \frac{(1-2\nu)}{E} \Delta \sigma_T - s \alpha_s \Delta T, \quad (28)$$

$$\Delta u_j = \frac{1}{k_n} \Delta \sigma_T \quad (29)$$

and  $\Delta \sigma_T$  = change in stress due to thermal effects. Noting that  $\alpha_s \Delta T = -1/3(\Delta v/v)$ , substituting equation (22) into (28) and substituting (28) and (29) into (27) gives:

$$\Delta \sigma_T = \left[ \frac{1}{k_n} + \frac{s(1-2\nu)}{E} \right]^{-1} \left( \frac{4\pi}{3} \right)^{1/3} \Delta u_a. \quad (30)$$

Total anticipated displacement of the joint may be directly evaluated from equation (26) as:

$$\Delta u_j = \left[ \frac{E}{s(1-2\nu)} + k_n \right]^{-1} (\Delta \sigma_T - \Delta p), \quad (31)$$

from which current aperture ( $b$ ) may be easily determined for any combination of stress level and appropriate joint normal stiffness ( $k_n$ ) such that  $b = b_r - \Delta u_j$ . Joint surface displacements are assumed positive in

closing. With the fissure apertures uniquely defined as a function of thermally induced displacements ( $u_a^t$ ), virgin field stresses ( $\sigma_i$ ), fracture spacing ( $s$ ), rock mass elastic constants ( $E, \nu, k_n$ ) and residual aperture ( $b_r$ ) the hydraulic conductivity of the system may be evaluated. Choosing the parallel plate analogy without modification for fracture wall roughness, the hydraulic conductivity of a ubiquitously jointed medium of isotopic fracture aperture ( $b$ ) is:

$$K_f = \frac{gb^3}{6\nu_r s}, \quad (32)$$

where  $\nu_r$  = fluid kinematic viscosity and  $g$  = gravitational acceleration. This completes the definition of all factors strongly influencing the flow regime.

#### ASSUMPTION OF FULL LATERAL RESTRAINT

The assumption of full lateral restraint requires that global strains within the rock mass are zero. This constraint, however, does not preclude thermal contraction of individual rock blocks and complementary opening of fractures. Because stresses within adjacent control volumes are modified independently and as a consequence of thermal stressing and fluid pressurization, only, force equilibrium is not globally maintained. Displacement compatibility in both the local and global sense is enforced as is consistency between local stresses, displacements and the constitutive model for the jointed medium.

The approximations posed within the assumption are no more onerous than those embodied within the storativity concept utilized in groundwater hydrology. The storativity of a medium describes the rate at which fluid is expelled from a differential volume element under a rate change in fluid pressure. No attempt is made to simultaneously satisfy displacement compatibility between adjacent differential elements since the flow problem is fully decoupled from the displacement field. Storativity concepts have been shown to function adequately where induced displacements are necessarily small. A direct analogy may be drawn with the full lateral restraint assumption; where stress redistribution resulting from thermal effects is not massive, the assumptions appear quite reasonable.

#### FINITE ELEMENT FORMULATION

Returning to the governing equations (1) and (2), the unknown terms anticipated to most greatly affect energy transfer within the system, are fully defined. Formation hydraulic conductivity  $K_f$ :

$$K_f = f(T_f(t), \alpha_s, \sigma_i, E, \nu, k_n, s, b_r) \quad (33)$$

and heat flux from the solid phase  $q_s$ :

$$q_s = f(T_f(t), D_s, \rho_s, c_s, s) \quad (34)$$

are functions of the above parameters. The governing partial differential equations may be solved most conve-

niently by using a finite element scheme. Normal Galerkin weighting is applied to the mass balance equation [equation (1)] and upstream weighting [9] is applied to the energy balance equation [equation (2)]. Analysis by this procedure is well known and will not be further described here. Equations (1) and (2) may be defined, respectively, at the local elemental scale as:

$$\mathbb{K} \mathbf{p}_f^t + \mathbb{S} \dot{\mathbf{p}}_f^t = \mathbf{q}_f^t, \quad (35)$$

$$[\mathbb{D} + \mathbb{E}] \mathbf{T}_f^t + \mathbb{F} \dot{\mathbf{T}}_f^t = \mathbb{G} \mathbf{q}_s^t, \quad (36)$$

where  $\mathbb{K}$  = fluid conductivity matrix,  $\mathbb{S}$  = fluid storativity matrix (lumped),  $\mathbb{D}$  = thermal diffusion matrix,  $\mathbb{E}$  = thermal advection matrix,  $\mathbb{F}$  = thermal heat capacity matrix (consistent),  $\mathbb{G}$  = rock thermal capacity matrix (consistent),  $\mathbf{P}_f$  = nodal fluid pressure vector,  $\mathbf{q}_f$  = nodal fluid discharge vector,  $\mathbf{T}_f$  = nodal fluid temperature vector,  $\mathbf{q}_s$  = nodal thermal discharge vector. A dot superscript represents time derivatives and both equations are written at any time level  $t$ . For completeness, the form of the individual matrices representing a two noded plane flow or radial flow element are included in the Appendix.

Nodal variables for sequential time steps  $t^l$  and  $t^{l+1}$  may be written using finite differences via a Crank-Nicolson implicit scheme for equations (35) and (36) where:

$$\mathbf{P}_f^{l+1/2} = \frac{1}{2}(\mathbf{P}_f^l + \mathbf{P}_f^{l+1}) \quad (37)$$

and

$$\mathbf{T}_f^{l+1/2} = \frac{1}{2}(\mathbf{T}_f^l + \mathbf{T}_f^{l+1}). \quad (38)$$

Substituting equations (37), (38) and (18) into equations (35) and (36) and rearranging yields the final system of equations:

$$\begin{aligned} & \left[ \frac{1}{2} \mathbb{K}(T) + \frac{1}{\Delta t} \mathbb{S} \right] \mathbf{P}^{l+1} \\ & = \left[ \frac{1}{\Delta t} \mathbb{S} - \frac{1}{2} \mathbb{K}(T) \right] \mathbf{P}^l + \frac{1}{2} [\mathbf{q}_f^l + \mathbf{q}_f^{l+1}], \quad (40) \end{aligned}$$

$$\begin{aligned} & \left[ \frac{1}{2} (\mathbb{D} + \mathbb{E}) + \frac{1}{\Delta t} \mathbb{F} - \mathbb{G} \mathbf{B}_1^{l+1} \right] \mathbf{T}_f^{l+1} \\ & = \left[ \frac{1}{\Delta t} \mathbb{F} - \frac{1}{2} (\mathbb{D} + \mathbb{E}) + \frac{1}{2} \mathbb{G} (\mathbf{B}_1^l - \mathbf{B}_1^{l+1}) \right] \mathbf{T}_f^l \\ & \quad - \frac{1}{2} \mathbb{G} \mathbf{B}_1^l \mathbf{T}_f^{l-1} + \frac{1}{2} \mathbb{G} [\mathbf{B}_2^l + \mathbf{B}_2^{l+1}], \quad (41) \end{aligned}$$

where hydraulic conductivity  $\mathbb{K}(T)$  is temperature history dependent. The content of vectors  $\mathbf{B}_1$  and  $\mathbf{B}_2$  follows directly from equation (18). These coupled equations are solved iteratively within each time step to describe thermal porosity changes within the formation.

#### VALIDATION STUDIES

The capabilities of the upwind weighting scheme used in the finite element formulation have been well demonstrated in cases where advective transport processes

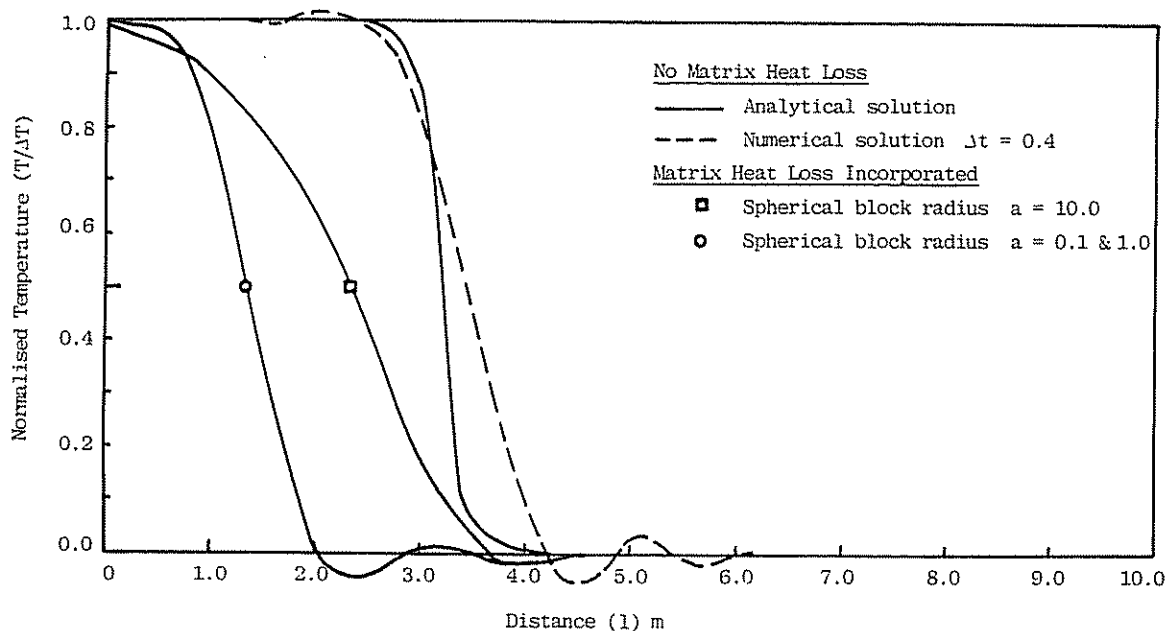


Fig. 4. Validation results for plane flow at a Peclet Number ( $P_e$ ) of 100. Results from the upwind finite element solution are illustrated for the validated case with no matrix heat loss and for different sized matrix blocks. Numerical parameters  $q/\phi = 0.5$ ;  $D_f = 0.0025$ ;  $\Delta t = 0.4$ ;  $t = 6.4$ ;  $l =$  element length  $= 0.5$ ;  $D_f/\rho_f c_f =$  matrix thermal diffusivity  $= 1$ .

dominate. The dominance of advective transport over diffusive transport is best referenced with respect to the Peclet Number ( $P_e$ ) where, at the local element level:

$$P_e = \frac{q_f l \rho_f c_f}{\phi D_f} \quad (41)$$

and  $l$  is the element length. For cases where matrix thermal diffusion is neglected, a comparison of the numerical scheme with the results from an analytical solution [10] are illustrated in Fig. 4. Even for the relatively high Peclet Number of 100 the numerical results show minimal overshoot, undershoot and smearing of the thermal front.

Where thermal diffusion into the surrounding rock mass (initially at a reference temperature of zero) is accommodated, the sharpness of the thermal front will be diffused. This effect is also illustrated in Fig. 4 where the effects of three different fracture spacings are examined. As would be expected, where the dimensions of individual blocks are small, the rapidity with which the percolating fluid is cooled is most marked. This is due to both the high specific surface area ratio of the smaller blocks and the short heat transfer length afforded by the blocks. Although, from Fig. 4, it is evident that the larger blocks are less efficient in cooling the passing fluid in the short term, the extended duration of the block thermal flux maintains inlet fluid temperatures lower for large blocks versus the smaller blocks.

#### PARAMETRIC STUDIES

Although equally applicable for 1-D or radial flow, the following suite of numerical tests are completed for a 1-D flow domain. This geometry is chosen to demonstrate the manner in which a number of fundamental processes are observed to operate in the absence of

considering the divergent flow field and resulting velocity distribution of radial flow. The chosen geometry is one of flow within a 200-m long plane section within a blocky granite rock mass. Appropriate material parameters, consistent with both the Camborne and Fenton Hill HDR sites, are documented in Table 1. The initial stress field is assumed uniform at 10 MPa and a uniform initial joint aperture of 0.02 mm is chosen to bound individual blocks. To this initially uniform system plane flow is induced at a pressure of 1 MPa above the initial ambient groundwater pressure. The percolating fluid is 10°C cooler than the fluid initially saturating the rock mass. A total of 20 elements are used in all analyses corresponding to a maximum block size to element length ratio ( $s/l$ ) of 1:1. The minimum ratio is  $10^{-2}$ . Flow velocities are evaluated by accounting for the variation in porosity with time but do not include the influence of temperature dependent viscosity.

Over the stable time step increment ( $\Delta t$ ) of  $10^4$  sec the flow system equilibrates to yield a steady state uniform pressure drop between influent and effluent points in the

Table 1. Model parameters

Factured granite at 400 m depth, initial stresses $\sigma = 10$ MPa	
Granite	
Density ( $\rho_s$ ) [11]	2627 kg/m <sup>3</sup>
Poisson Ratio ( $\nu_s$ ) [11]	0.22
Deformation modulus ( $E_s$ ) [12]	$58 \times 10^3$ MPa
Specific heat ( $c_s$ ) [11]	918 J/kg °C
Coefficient of thermal expansion ( $\alpha_s$ ) [11]	$7.42 \times 10^{-6}/^\circ\text{C}$
Thermal conductivity ( $D_s$ ) [11]	9770 J/hr·m·°C
Joint normal stiffness ( $k_n$ ) [12]	$10^5$ MPa/m
Fluid:	
Density ( $\rho_f$ ) [13]	1000 kg/m <sup>3</sup>
Specific heat ( $c_f$ ) [13]	4187 J/kg °C
Thermal conductivity ( $D_f$ ) (@ 75°C) [13]	2262 J/hr·m·°C
Compressibility ( $\beta_f$ ) [14]	$0.4239 \times 10^{-3}$ MPa <sup>-1</sup>
Kinematic viscosity ( $\nu_f$ ) [14]	0.0029 m <sup>2</sup> /hr

Table 2. Stress and displacement response of a thermally equilibrated system

Block size (m)	10	1	0.1
Thermal stress change $\Delta\sigma_T$ (MPa/°C)	0.697	0.338	0.042
Joint aperture increase $\Delta u_j$ (mm/MPa)	0.0090	0.0049	0.0009

plane flow system. This steady pressure distribution corresponds to a flow velocity of  $0.2 \times 10^{-3}$  m/sec as representative of the initial, isothermal system.

The projected deformation and stress change behaviour of the rock mass under uniform and equilibrium thermal loading conditions is summarized in Table 2. It is apparent from this that the largest changes in thermal stress will result from the mass containing the largest joint spacing. Similarly, expected aperture changes resulting from thermal stresses are greater for the larger joint spacings.

The form of the thermal flow fields after an elapsed time of 2.3 days are shown in Fig. 5 for the case of 10-m spacing between joints. Illustrated are the three cases where: (i) heat transfer is not accommodated between rock and fluid and thermal fissure aperture enhancement is suppressed; (ii) heat transfer is not accommodated between rock and fluid, and aperture change is manifest; and finally (iii) where the fully interactive system is monitored with both permeability enhancement and thermal diffusion effects present. The sharpest thermal front is apparent where no thermal diffusion occurs. Fluid temperatures close to the inlet are coolest for the greatest transit length. The effect of diffusion is to marginally warm the water at inlet, this comparison being most evident for the case where no aperture enhancement occurs. The numerical undershoot observed at the tip of the thermal front is damped by the

influence of rock mass diffusion, thus reducing the magnitude of spurious positive temperature readings. Where both permeability enhancement and thermal diffusion effects are accommodated, the position of the thermal front is accelerated over that where neither of these factors are considered. Aperture changes apparently diffuse the sharp thermal gradients at the thermal interface. A portion of this diffusion may result from the upwind weighting. The position where the fluid temperature is half that of inlet temperature ( $T_{50}$ ) is advanced by approx. 35% over the cases where aperture enhancement effects are suppressed.

As the thermal system further develops, the fluid temperature profiles after an elapsed time of 4.6 days are illustrated in Fig. 6. As a more developed case than that from the previous time window at  $t = 2.3$  days, the non-diffusive case exhibits the sharpest thermal front and diffusion effects are again shown to reduce spurious undershoot. Where no aperture change is accommodated, the resulting lower velocity and volumetric flows further increase the lag of fluid temperatures behind the thermal crest between the ordinates of 40 and 70 m. Where aperture changes are apparent, thermal diffusion or smearing at the front are more developed than at  $t = 2.3$  days. The lateral separation between the mid temperature locations of the thermal front ( $T_{50}$ ) for the rigid and aperture enhanced cases after a time of 2.3 and 4.6 days has increased from a 35% difference to one greater than 50%. This effect is a combined result of both the continual downflow direction changes in aperture as the thermal front proceeds and due to time delay in the development of aperture changes in any one location. The latter of these effects is highlighted in Table 3 where the displacement reaction times for different block dimensions ( $s$ ) are described. For a joint spacing ( $s$ ) of 10 m, the time to reach 50% displacement follow-

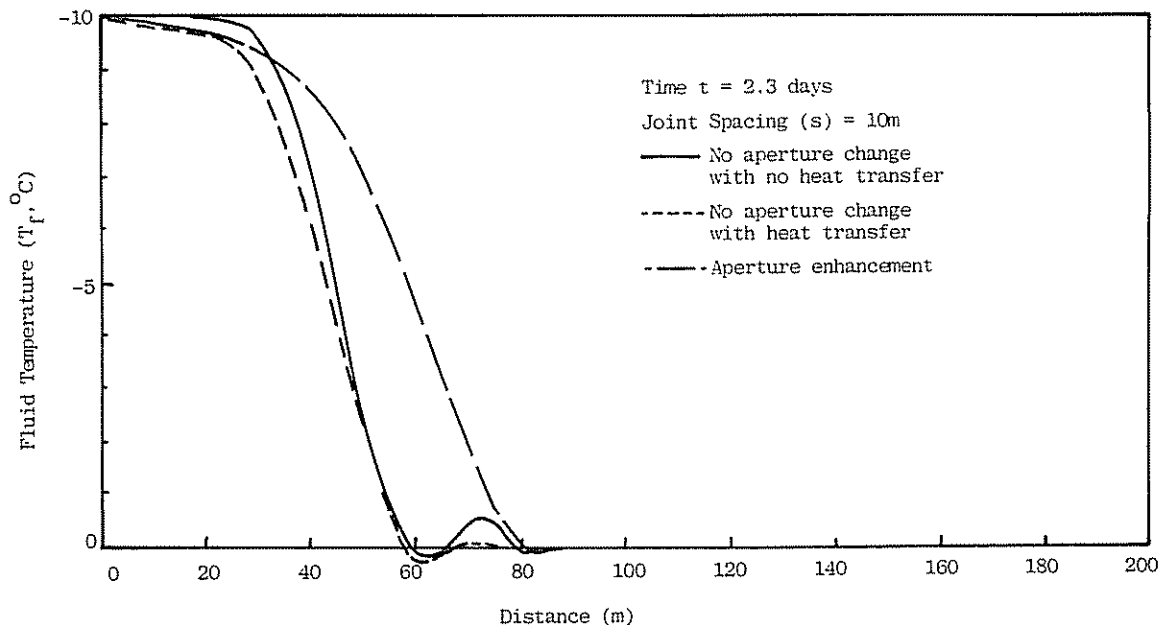


Fig. 5. Fluid temperature profiles for plane flow after 2.3 days. Fluid temperature 10°C cooler than rock; fluid pressure drop 1 MPa along 200 m flow path;  $\Delta t = 10,000$  sec; fracture spacing ( $s$ ) = 10 m.

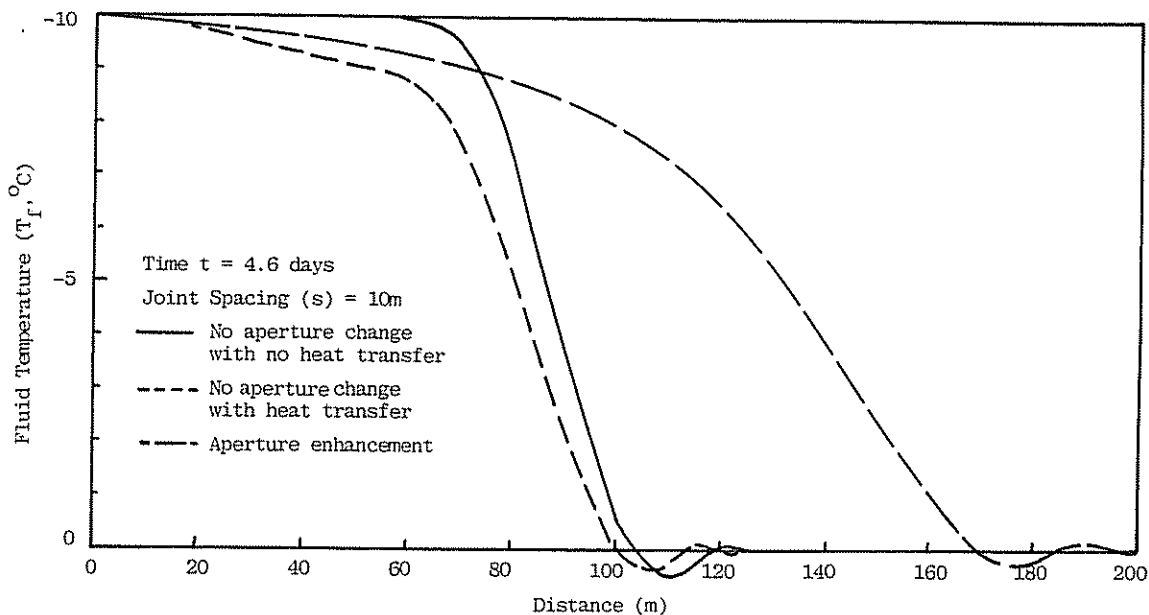


Fig. 6. Fluid temperature profiles for plane flow after 4.6 days. Fluid temperature  $10^{\circ}\text{C}$  cooler than rock; fluid pressure drop 1 MPa along 200 m flow path;  $\Delta t = 10,000$  sec; fracture spacing ( $s$ ) = 10 m.

ing an initial change in temperature at the block surface is 11.86 days. This compares with a 50% equilibration time for a smaller 0.1 m block of 1.7 min. Of critical importance here is that displacement response is proportional to block dimension raised to the power two. A further reason for acceleration of the thermal front with elapsed time is that flow velocity is proportional to the squared aperture. Thus, small aperture changes geometrically increase flow velocities which correspondingly increase propagation rates.

Where block dimensions are decreased by two orders of magnitude to a joint spacing ( $s$ ) of 0.1 m, propagation rate through the system is correspondingly reduced. Results for this case are illustrated in Fig. 7 at time levels  $t = 2.3$  and  $t = 4.6$  days where heat transfer and aperture enhancement are again systematically examined. Rock mass thermal diffusion effects are more pronounced as joint spacing decreases and the resulting specific fracture surface area increases. Heat transfer rate from the rock to the fluid is further increased by the shortening of the diffusion path to the fracture allowing more rapid thermal depletion of the rock blocks. These effects are manifest as a greater difference between the results for the non-diffusive and diffusive cases as shown in Fig. 7. Similarly apparent from the results is that both aperture enhancement and thermal stress change magnitudes are reduced for the smaller block size as is apparent from Table 2. Indeed, at this block dimension, thermal changes appear to little influence the flow regime. The parallel form of the thermal fronts suggest that thermal depletion occurs rapidly as fluid passes through the fractured mass.

Coupling within the flow and transport system is via velocity changes within the fluid phase. The progression of changes within the flow field effected by thermal transport are most conveniently illustrated through observing the development of spatial changes in fluid pressure. The nature of the flow system chosen in this

example is such that it effectively reaches a steady condition over the period of successive iterative time increments ( $\Delta t$ ). Pressure changes that develop with the mechanism of thermal transport are illustrated in Fig. 8 for the three block dimensions ( $s$ ) of 0.1, 1 and 10 m at time  $t = 4.6$  days. With no aperture change, the pressure drop between inlet and outlet is linear. This linear distribution is most affected by aperture enhancement close to the inlet for the larger block spacings. As has already been established, aperture changes possible for large block dimensions greatly exceed those for smaller blocks. The concave downwards form of the pressure profile suggests downstream tapering of the fracture system with greater pressure loss close to the outlet. Interestingly, the pressure distributions for 1 and 10-m blocks are similar at inlet before they diverge downflow. Although ultimate aperture enhancement will be greater for the larger block (see Table 2), the reaction time of the smaller block is more swift [Table 3;  $t_{50} = 11.9$  days (10 m) vs 2.8 hr (1 m)]. These effects apparently cancel at small times. The greater propagation velocity of the thermal front in the case of the larger block size results in greater downflow aperture enhancement and a corresponding reduction in pressure loss.

A minimal pressure change is effected for the smaller block dimension of ( $s$ ) 0.1 m. If the temperature differential at inlet is increased from  $-10$  to  $-20^{\circ}\text{C}$ , a slightly greater permeability enhancement occurs at inlet. For the relatively small stress changes precipitated as a result of thermal displacement in this instance, the fluid pressure gradient is likely to have a more significant

Table 3. Block displacement response rate

Block size (m)	10	1	0.1
$t_{50}^*$	11.9 days	2.84 hr	1.7 min
$t_{95}$	102.8 days	24.67 hr	14.8 min

\* $t_{50}$  = time to reach 50% of maximum displacement following instantaneous loading.

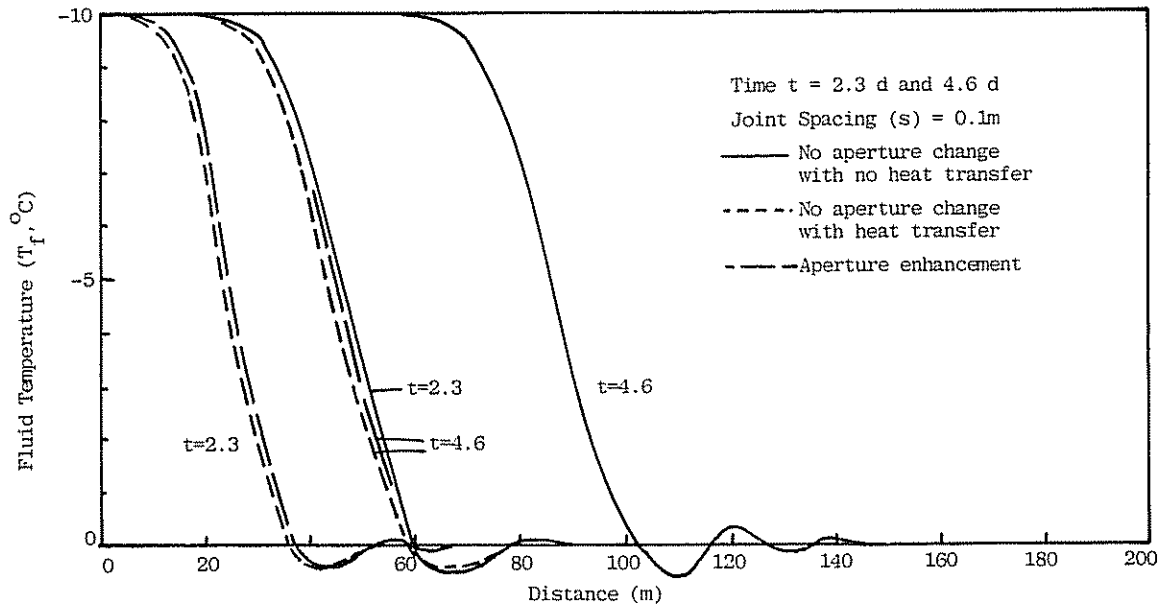


Fig. 7. Fluid temperature profiles for plane flow with fracture spacing ( $s$ ) = 0.1 m. Time = 2.3 and 4.6 days.

influence on aperture enhancement than temperature change.

The propagation of a thermal front within the fluid at successive time intervals for a block dimension ( $s$ ) of 1 m is illustrated in Fig. 9. As time progresses, the front becomes more diffuse as the influence of aperture enhancement becomes more pronounced. This transient thermal record may be used to explain the temporal change in pressure distribution along the fracture, as illustrated in Fig. 10. At the onset of flow ( $t = 2.3$  and 4.6 days), aperture changes close to the inlet produce a local reduction in pressure gradient with a corresponding increase in pressure gradient downflow. These changes become more pronounced as the thermal front propagates ( $t = 6.9$  and  $t = 9.2$  days). Ultimately, however, as the thermal front reaches the outlet ( $t = 9.2$  days+) the

concave downward pressure profile abates as the difference between inlet and outlet aperture is reduced. In this case (see Table 3), the block reaction time to reach 95% of ultimate displacement is only of the order of 1 day and this relatively rapid response is the primary cause of the timely pressure abatement.

CONCLUSIONS

Subject to the validity of the initial assumptions of full lateral restraint, thermally induced displacements within geothermal systems may have significant effects on temporal and spatial pressure drop and flow impedance characteristics of cooled rock reservoirs. The following conclusions may be drawn:

- (a) Thermal diffusion between solid and fluid phases

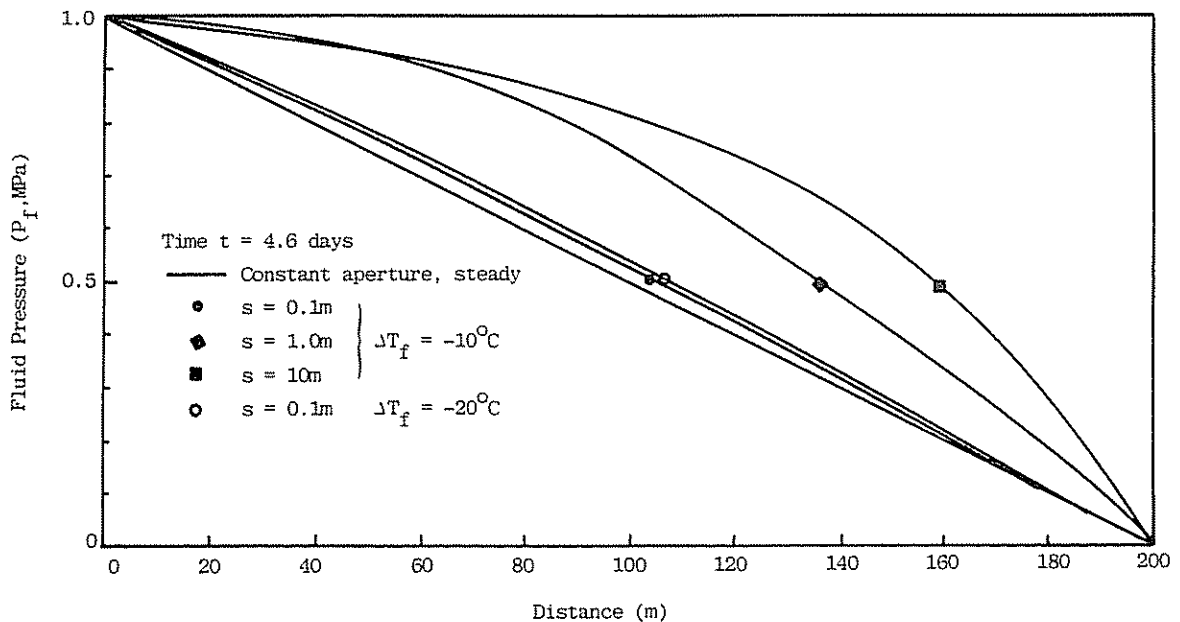


Fig. 8. Variation in fluid pressure ( $P_f$ ) along flow system axis at time  $t = 4.6$  days for fracture spacing ( $s$ ) = 0.1, 1 and 10 m.

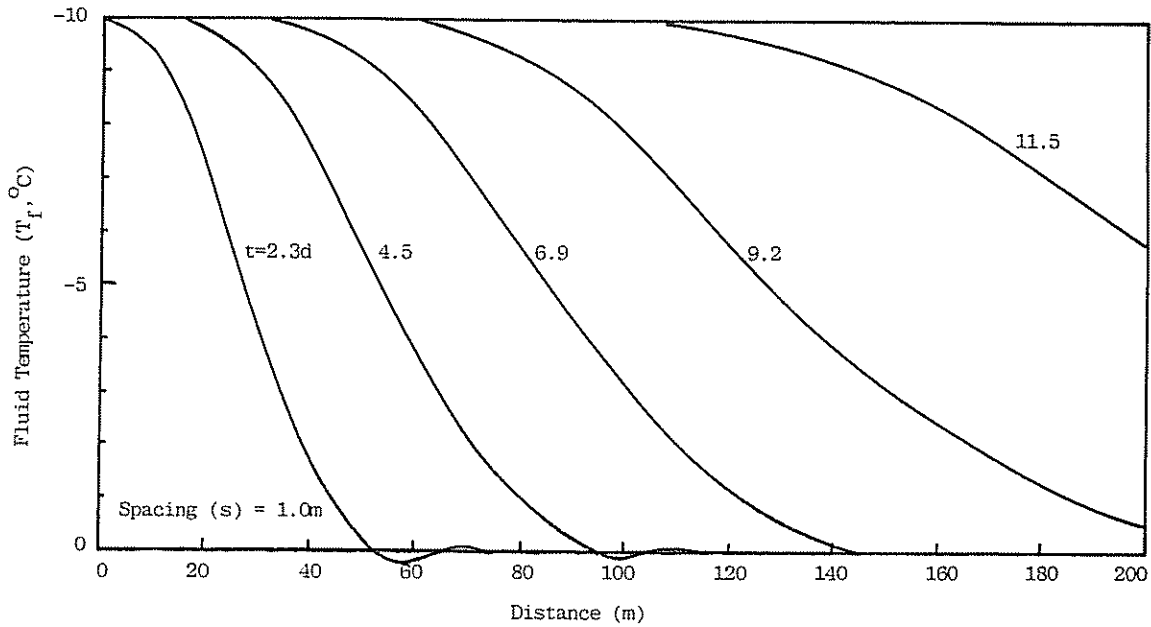


Fig. 9. Thermal propagation within the flow system for fracture spacing ( $s$ ) = 1 m at times  $t$  = 2.3, 4.6, 6.9, 9.2 and 11.5 days.

- accommodated in the model is a significant phenomenon, the most prominent effects of which are evident at early times for small rock block dimensions. This behaviour is conditioned by the increase in specific area that accompanies the accelerated response rate of smaller blocks.
- (b) Joint aperture changes resulting from both fluid pressure and thermal effects are more pronounced with increased block dimension. This behaviour is, in part, a function of the assumption of full lateral restraint and may result in significantly shorter transit and breakthrough times for the thermal front over the case where thermal displacement effects are not considered.

These effects seem significant even for modest temperature changes of the order of  $10^{\circ}\text{C}$ .

- (c) In addition to accelerating the transit of a thermal pulse, aperture enhancement causes a significant diffusion of the initially sharp interface between initially warm and penetrating cold fluids.
- (d) The pressure gradients that control flow in the fracture system are affected in a transient manner by the propagating thermal disturbance.

Changes in permeability induced by relatively modest temperature modifications appear significant. These effects may be an important consideration in both the analysis of pumping tests within blocky rock systems

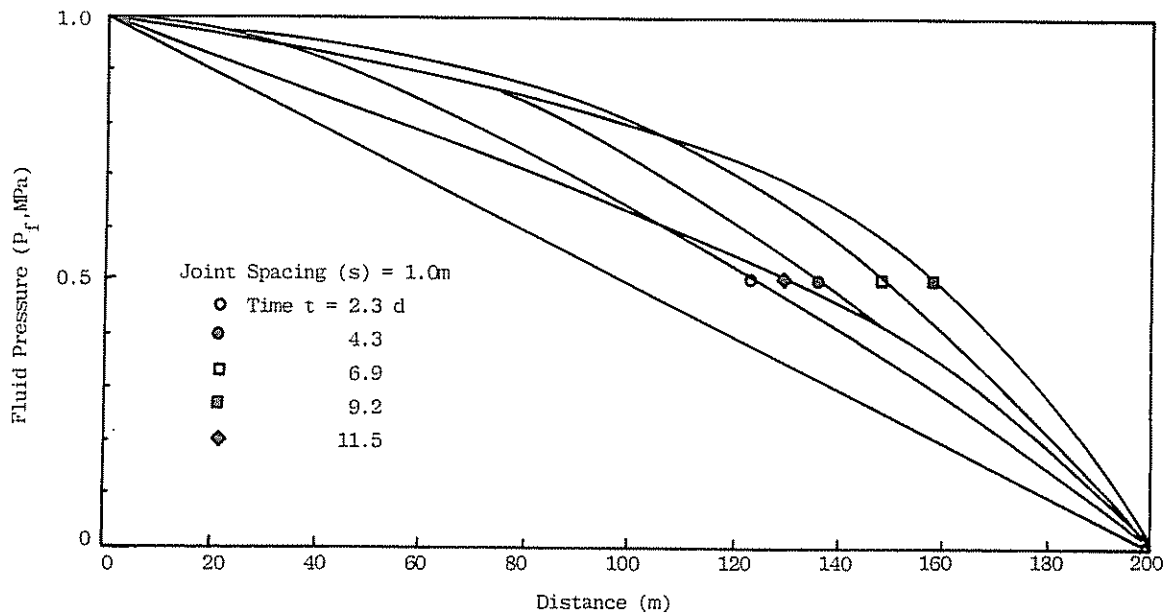


Fig. 10. Variation in fluid pressure ( $P_f$ ) along flow system axis for joint spacing ( $s$ ) = 1 m and time  $t$  = 2.3, 4.6, 6.9, 9.2 and 11.5 days.

and in planning the development of hot dry rock and other geothermal energy schemes where the induced flow system is advection dominated. Correct interpretation of pumping tests conducted, unwittingly, under non-isothermal conditions and optimal development of geothermal reservoirs require cognizance and quantification of these influencing factors.

*Acknowledgement*—This work was sponsored by the Engineering Foundation under Grant RI-A-86-13. This support is most gratefully acknowledged.

REFERENCES

1. Murphy H. Hot dry rock reservoir development and testing in the U.S.A. *Proc. 1st Japan-U.S. Seminar on Hydraulic Fracturing and Geothermal Energy*, pp. 33-38. Martinus Nijhoff, (1982).
2. Brekke T. L., Noorishad J., Witherspoon P. A. and Maini Y. N. T. Coupled stress and flow analysis of fractured dam foundations and rock slopes. *Proc. Symp. on Percolation Through Fissured Rock*, Stuttgart, T4-J, pp. 1-7 (1972).
3. Pine R. J. and Cundall P. A. Applications of the fluid-rock interaction program (FRIP) to the modelling of hot dry rock geothermal energy systems. *Proc. Int. Symp. on Fundamentals of Rock Joints*, pp. 293-302. Centek (1985).
4. Nemat-Nasser S. Thermally induced cracks and heat extraction from hot dry rocks. *Proc. 1st Japan-U.S. Seminar on Hydraulic Fracturing and Geothermal Energy*, pp. 11-31. Martinus Nijhoff, The Hague (1982).
5. Boley B. A. and Weiner J. H. *Theory of Thermal Stress*, p. 586. Wiley, New York (1960).
6. Carslaw H. S. and Jaeger J. C. *Conduction of Heat in Solids*, Second Edn, p. 510. Oxford University Press (1959).
7. Bibby R. Mass transport of solutes in dual porosity media. *Water Resources Res.* 17, 1075-1081 (1981).
8. Huyakorn P. S., Lester B. H. and Faust C. R. Finite element techniques for modeling groundwater flow in fractured aquifers. *Water Resources Res.* 19, 1019-1035 (1983).
9. Christie I., Griffiths D. F., Mitchell A. R. and Zienkiewicz O. C. Finite element methods for second order differential equations with significant first derivatives. *Int. J. Numer. Method. Engng* 10, 1389-1396 (1976).
10. Nooishad J. and Mehran M. An upstream finite element method for solution of transient transport equation in fractured porous media. *Water Resources Res.* 18, 588-596 (1982).
11. Kruger P. Experimental studies on heat extraction from fractured geothermal reservoirs. *Proc. First Japan-U.S. Joint Seminar on*

*Hydraulic Fracturing and Geothermal Energy*, Tokyo, Japan. Martinus Nijhoff, The Hague (1982).

12. Iwai K. Fundamental studies of fluid flow through a single fracture. Ph.D. Thesis, University of California, Berkeley, p. 208 (1976).
13. Bennett C. O. and Myers J. E. *Momentum, Heat and Mass Transfer*, Third Edn. McGraw-Hill, New York (1982).
14. Daugherty R. L. and Franzini J. B. *Fluid Mechanics with Engineering Applications*. Seventh Edn, McGraw-Hill, New York (1977).

APPENDIX

The elemental matrices for a radial, two-noded element are as follows:

$$\begin{aligned}
 \mathbb{D} &= \int_0^{2\pi} \int_{r_1}^{r_2} \mathbb{W}^T (D_t/\phi) \mathbb{N} r dr d\theta, \\
 \mathbb{E} &= \int_0^{2\pi} \int_{r_1}^{r_2} \rho c_f (q_t/\phi) \mathbb{W}^T \mathbb{N} r dr d\theta, \\
 \mathbb{F} &= \int_0^{2\pi} \int_{r_1}^{r_2} \mathbb{W}^T \mathbb{N} r dr d\theta, \\
 \mathbb{G} &= \int_0^{2\pi} \int_{r_1}^{r_2} \mathbb{W}^T \mathbb{N} r dr d\theta, \\
 \mathbb{K} &= \int_0^{2\pi} \int_{r_1}^{r_2} \frac{1}{\gamma_t} \mathbb{N}^T K_r \mathbb{N} r dr d\theta, \\
 \mathbb{S} &= \int_0^{2\pi} \int_r \phi \beta_f \mathbb{N}^f \mathbb{N} r dr d\theta,
 \end{aligned}$$

and

$$\begin{aligned}
 x &= r - r_1, \\
 l &= r_2 - r_1, \\
 \mathbb{N} &= \left[ 1 - \frac{x}{l}; \frac{x}{l} \right]; \mathbb{N} = \frac{\partial}{\partial x} \mathbb{N}, \\
 \mathbb{W} &= \left[ 1 - \frac{x}{l} + 3\alpha \left( \frac{x^2}{l^2} - \frac{x}{l} \right); \frac{x}{l} - 3\alpha \left( \frac{x^2}{l^2} - \frac{x}{l} \right) \right]; \\
 \mathbb{W} &= \frac{\partial}{\partial x} \mathbb{W},
 \end{aligned}$$

where  $\alpha$  is positive for flow directed in the positive  $r$  direction, negative for flow directed in the negative  $r$  direction and  $0 < |\alpha| < 1.0$ . For 1-D flow the matrix expressions are pre-divided by  $r$  and the integration over  $\theta$  is eliminated.

